Experimental Observations of Mode-Converted Ion Cyclotron Waves in a Tokamak Plasma by Phase Contrast Imaging

E. Nelson-Melby,* M. Porkolab, P. T. Bonoli, Y. Lin, A. Mazurenko, and S. J. Wukitch

Plasma Science and Fusion Center, Massachusetts Institute of Technology, Cambridge, Massachusetts 02139

(Received 13 September 2002; published 18 April 2003)

The process of mode conversion, whereby an externally launched electromagnetic wave converts into a shorter wavelength mode(s) in a thermal plasma near a resonance in the index of refraction, is particularly important in a multi-ion species plasma near the ion cyclotron frequency. Using phase contrast imaging techniques (PCI), mode-converted electromagnetic ion cyclotron waves have been detected for the first time in the Alcator C-Mod tokamak near the H-^{3}He ion-ion hybrid resonance region during high power rf heating experiments. The results agree with theoretical predictions.

DOI: 10.1103/PhysRevLett.90.155004 PACS numbers: 52.35.Hr, 52.50.Qt, 52.55.Fa, 52.70.Kz

Mode conversion of an externally launched long wavelength electromagnetic wave into shorter wavelength electromagnetic or electrostatic waves is an important physical phenomenon that may occur in a finite temperature, inhomogeneous, anisotropic plasma when under similar conditions cold plasma (or MHD) theory would predict a resonance in the index of refraction. The basic theory was worked on originally by Budden [1] and Stix [2]. The problem is of particular importance for rf heating in fusion plasmas near the ion cyclotron range of frequencies (ICRF) in a multi-ion species plasma where the ion-ion hybrid resonance (located between the ion cyclotron frequencies of a particular ion species pair) plays an important role. At such a layer, the incident fast magnetosonic wave (used to heat the plasma by ion cyclotron absorption on one of the ion species) may be converted into a short wavelength electrostatic ion Bernstein wave (IBW) [3–6] or the electromagnetic slow ion cyclotron wave (ICW) [3]. While in a slab geometry the former process dominates [5,6], in the presence of the sheared magnetic field of a tokamak geometry mode conversion into the ICW may dominate [3]. In this Letter we present experimental results that verify for the first time that the ICW plays a dominant role for typical tokamak plasma parameters, in agreement with theoretical predictions of Perkins [3]. A similar phenomenon may occur in D-T fusing plasmas during ICRF heating with a profound influence on the resulting heating profiles and transport of energy and particles.

More recently, the problem has been studied in tokamak geometry by using large, computationally intensive full-wave codes [7–9]. Previous attempts to measure mode-converted waves in magnetic fusion experiments have relied on small-angle laser scattering (CO_2 or far-infrared) [10–12] or microwave scattering [13]. These techniques are limited in observation volume and wave number range. The phase contrast imaging (PCI) diagnostic [14,15] allows the observation of a large region of the radial plasma cross section and a wide range of wave numbers simultaneously, but gives no information on spatial localization of the waves along the laser beam. Nevertheless, PCI allows a more complete mapping of the mode-conversion region, including both short and long wavelength modes, improving the understanding of the mode-conversion process.

This Letter presents experimental investigation results of mode conversion in multi-ion species (H-D-^{3}He) plasmas in the Alcator C-Mod tokamak [16] using a phase contrast imaging technique. A mode with wavelengths (1–2 cm) intermediate between typical IBW (~3 mm) and FW (~10 cm) dominates the measured scattered wave spectrum. This mode propagates to the low-field side (larger major radius R) of the H-^{3}He ion-ion hybrid layer. The measured wave numbers and spatial amplitude distribution in the mode-conversion region agree with the TORIC code simulation [9]. We have numerically evaluated a full electromagnetic dispersion relation [2] to identify the detected waves as mode-converted ICWs propagating to the low-field side of the ion-ion hybrid layer. The existence of this intermediate wavelength mode was first derived by Perkins who showed that in a 1D model, including the poloidal magnetic field, mode conversion into ICWs can dominate in a D-T plasma (same ratio of cyclotron frequencies as our H-^{3}He plasma) depending upon species mix [3]. In both the simulation and evaluation of the dispersion relation, the sheared magnetic field plays a crucial role in the mode-conversion process. High poloidal mode numbers (m_θ) in the mode-converted wave fields are converted to large parallel wave numbers ($k_\parallel$) via the shear, resulting in significant modification to the topology of the mode-conversion region.

Figure 1 illustrates a typical case where the FW and ICW wave numbers coincide at the mode-conversion layer, using a set of plasma parameters representative of these 3-species plasmas: toroidal magnetic field at the center ($R = R_0 = 67$ cm) $B_\phi = 5.8$ T, plasma current $I_p = 800$ kA, ion species mix 33% H, 23% ^{3}He, 21% D, $n_e = 2.4 \times 10^{20}$ m^{-3}, $T_e = T_i = 1.5$ keV (ion densities are normalized to the electron density, so multiply by charge state to sum to 100%). The mode-conversion layer

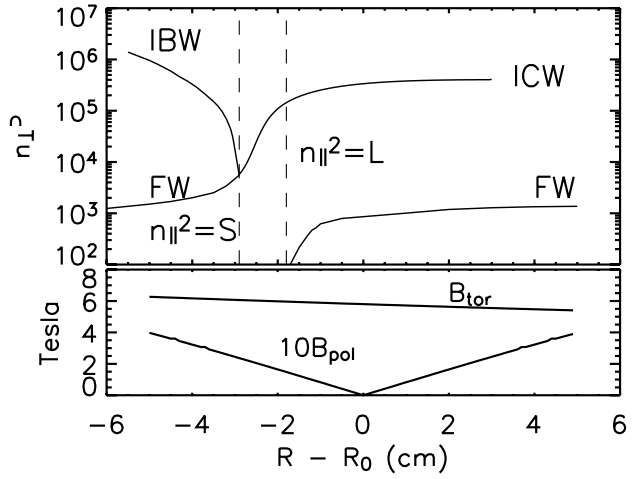

FIG. 1. (a) Top: $n_\perp^2 = c^2k_\perp^2/\omega^2$ vs $R - R_0$ for the fast wave (FW), ion cyclotron wave (ICW), and ion Bernstein wave (IBW). The FW cutoff $n_\parallel^2 = L$ and mode conversion layer $n_\parallel^2 = S$ are also shown. (b) Bottom: Magnetic field profiles for toroidal and 10 times the poloidal field.

is defined as the location where $n_\parallel^2 = S$, with $n_\parallel = ck_\parallel/\omega$, and $S = 1 - \sum \omega_p^2/(\omega^2 - \Omega_c^2)$ is the Stix dielectric tensor element [2], the sum is over plasma species, ω_p is the plasma frequency, Ω_c is the cyclotron frequency, and the wave frequency is $\omega/2\pi = 80$ MHz. The ion-ion hybrid resonance shown in Fig. 1 is between the H and ^{3}He cyclotron resonances (located at 7.1 and -17.6 cm, respectively). The deuterium is not necessary for this kind of mode conversion, but its presence was required in order to move the mode-conversion layer closer to the center of the plasma (and the PCI viewing volume) for the available maximum magnetic field of 6 T in this series of experiments. For a given toroidal mode number n_ϕ and poloidal mode number m_θ, the parallel wave number can be expressed as $k_\parallel = (n_\phi B_\phi/R + m_\theta B_\theta/r)/|B|$, where r is the minor radius, B_θ is the poloidal magnetic field, and $|B| = \sqrt{B_\phi^2 + B_\theta^2}$. The dispersion relation in Fig. 1(a) was calculated for $n_\phi = 13$ and $m_\theta = 0$ for the FW and IBW along the midplane. The magnetic field profiles along the midplane are shown in Fig. 1(b). The plasma density profile is usually fairly flat, and does not change significantly from its central value in the region of interest. The ICW root was solved for along a flux surface at $r = 3$ cm (hence at constant $B_\theta = 0.25$ T) with $n_\phi = 13$ and m_θ evolving as required to solve the dispersion relation simultaneously with the approximate relation between $k_\perp$ and $k_\parallel$ for constant n_ϕ:

$$k_\parallel = (n_\phi B_\phi/R + k_\perp B_\theta)/|B|. \quad (1)$$

Near the mode-conversion layer, the FW, IBW, and ICW share a wave number of approximately 2 to 3 cm^{-1}. According to the local dispersion relation, the IBW wavelength becomes shorter as it propagates away from the mode-conversion layer to the high-field side. The ICW propagates toward the low-field side [3], the wavelength becoming shorter, but not as short as the IBW.

Electron density fluctuations driven by ICRF waves have been studied with a PCI diagnostic on C-Mod [17,18]. The spatial structure and wavelength can be derived from the PCI results. The PCI technique [14] relies on the interference of scattered and appropriately phase-shifted unscattered radiation passing through a phase object such as a plasma (where electron density fluctuations cause the scattering). The C-Mod PCI system [see Fig. 2(a)] uses a 10.6 μm wavelength CO_2 laser, expanded to a width of 15 cm, passing through the central portion of a ~42 cm wide plasma. After passing through the plasma and reflecting from the phase plate (phase shifting the unscattered light by 90°), the laser light is imaged onto a 12 element HgCdTe photoconductive linear array. The system is sensitive to frequencies from 2 to 500 kHz, and can resolve wave numbers in the range $0.4\,\text{cm}^{-1} \leq k \leq 10\,\text{cm}^{-1}$. The diagnostic is most sensitive to perturbations whose surfaces of constant phase are aligned vertically with the laser beam, so waves propagating in the major radial direction $\vec{k} = \vec{k}_R$ are most easily detected.

To detect electron density fluctuations at the rf frequency (~ 80 MHz), the laser intensity is modulated at a frequency offset, typically ~0.3 MHz, from the rf frequency [15]. When the 80 MHz fluctuation in the plasma is illuminated by the 80.3 MHz modulated laser, the image intensity (which is the product of both) reveals a 300 kHz beat oscillation, the frequency at which the signal is detected. A Fourier transform of the raw PCI data converts time and space into the frequency and wave number domain. In the reported results, positive wave numbers indicate that the phase velocity is toward the antenna. The PCI diagnostic is absolutely calibrated before each discharge using a sound wave passing through

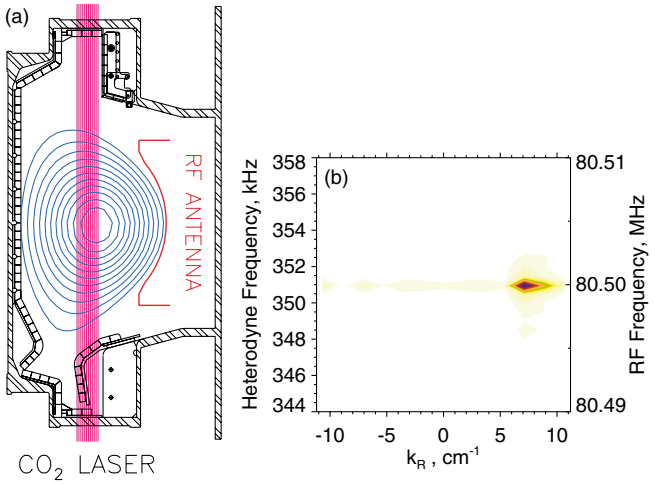

FIG. 2 (color online). (a) Left: The Alcator C-Mod tokamak cross section, with PCI laser path and rf antenna location shown. (b) Right: 2D Fourier transform of the PCI data, showing the presence of an ICW at the expected rf heterodyne frequency of 350.9 kHz.

air across the laser beam. Thus, the signal level can be related to the total line-integrated electron density perturbation in the plasma.

In these experiments, the plasma consists of roughly comparable amounts of D, ^{3}He, and H at a magnetic field of 5.8 Tesla. This places the mode-conversion region to the high-field side of center, with the location and mode-conversion efficiency depending sensitively on the exact species mix. Figure 2(b) gives an example of the Fourier-transformed PCI data, for a plasma discharge with the rf antenna driven at 80.5 MHz. The plasma parameters were $B_\phi = 5.84$ T, $I_p = 800$ kA, 59% H, 4% ^{3}He, 33% D, $n_e = 2.0 \times 10^{20}$ m^{-3}, $T_e = 1.3$ keV (the ion densities are only rough estimates). The phase advance from channel to channel of the Fourier-transformed 350.9 kHz harmonic was approximately the same across the 12 channels, accounting for the fairly narrow peak in k space. Typically, the measured wave numbers range from $+4$ to $+10$ cm^{-1}. The positive wave numbers indicate that the phase velocity is toward the low magnetic field side of the H–^{3}He hybrid resonance consistent with the expected ICW phase velocity.

Figure 3 gives an example of the scattered wave spectrum before and during the rf heating phase of a plasma discharge. Using experimentally estimated ^{3}He concentrations, the mode-conversion layer (defined by the condition $S = n_\parallel^2$ for $n_\phi = 10$, $m_\theta = 0$) is located at a major radius of 57 cm, far to the high-field side of the region monitored by the PCI. The plasma parameters were $B_\phi = 5.84$ T, $I_p = 1$ MA, 50% H, 8% ^{3}He, 34% D, $n_e = 2.5 \times 10^{20}$ m^{-3}, $T_e = 1.3$ keV. The short wavelength waves are observed to the low-field side of the ion-ion hybrid layer for all plasma conditions (varying ion concentrations and magnetic field) in the experiments reported here. This observation is in agreement with the location of the ICW predicted by Perkins [3]. The separation between amplitude peaks of 1 to 2 cm is longer than the typical IBW wavelength ($\sim$3 mm), yet shorter than the FW wavelength (or half-wavelength, typically 5 cm for these plasmas), again in agreement with the ICW dispersion relation. Figure 3 compares the wave structure to electron power deposition profiles determined from "break-in-slope" analysis of the electron temperature. There is strong electron heating in the vicinity of strong PCI signal as expected. The integrated electron power deposition profiles for these plasmas have shown experimentally that $\sim$20% to 50% of the total rf power is absorbed by electrons [19].

The detailed structure of the PCI signal intensity depends sensitively on the location of the mode-conversion region relative to the PCI laser and the mode-conversion efficiency, which both depend on the exact species mix, the electron density and its profile, and to a lesser extent on the temperature and magnetic field. To interpret the 1D PCI line-integrated measurements of an inherently 3D wave field structure, a sophisticated simulation code

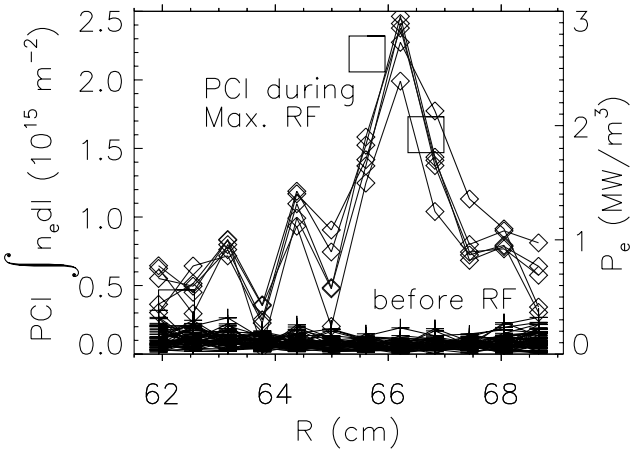

FIG. 3. Line-integrated PCI signal at the expected rf heterodyne frequency before (+) and during ($\diamond$) the application of rf power (scale on the left, 10^{15} m^{-2}). Also shown is the measured electron power deposition (large squares, scale on the right, MW/m^3). The magnetic axis is located at 67 cm, and the ion-ion hybrid layer is located to the high-field side of the plot, at 57 ± 2 cm.

(TORIC) [9] is used. TORIC solves for the field E_{RF} using a spectral ansatz of one toroidal mode number n_ϕ and many coupled poloidal mode numbers m_θ [all field quantities are assumed to be proportional to $\exp(in_\phi\phi + im_\theta\theta)$, where ϕ is the toroidal angle and θ the poloidal angle]. To resolve short wavelengths properly, 161 m_θ numbers are used. Using the electron fluid continuity equation and the linearized momentum conservation equation in the cold plasma limit, the solution for the rf fluctuating density n_{e1} can be solved in terms of E_{RF}, $\nabla \times E_{RF}$ (obtained from numerical differentiation of E_{RF}) and the total steady-state magnetic field, including B_ϕ and B_θ.

The full-wave ICRF code TORIC was run with the same set of plasma parameters as those associated with Fig. 1. Figure 4(a) shows the real part of the complex electron density fluctuation at $\phi = 0$ [n_{e1} is complex due to the $\exp(-i\omega t)$ dependence], calculated using the E_{RF} solution for $n_\phi = 13$. The region of short wavelength oscillation, representing the ICW, is to the low-field side of the fast wave mode-conversion layer for this n_ϕ, shown by the straight vertical dot-dash line.

In the TORIC simulations, IBW appears on the high-field side of the ion-ion hybrid layer, near the midplane. However, density fluctuations associated with the IBW are not present in Fig. 4(a) because they are much lower amplitude than the ICW. Although the electric field components perpendicular to the steady-state magnetic field can be roughly comparable for the IBW and ICW, the parallel electric field component $E_\parallel$ of the ICW dominates over that of the IBW. Because density fluctuations are more efficiently driven by $E_\parallel$, large density fluctuations are associated with the ICW but not IBW. For the experiments presented here, power balance studies also indicate that a majority of the mode-converted power ends up in

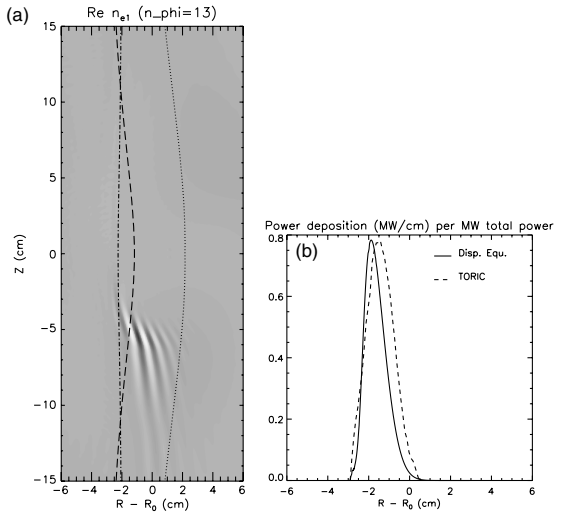

FIG. 4. (a) Left: Fluctuating rf density near the core of the plasma for $n_\phi = 13$, using data from the TORIC full wave code. (b) Right: Power deposition profile calculated using k_{im} from the full electromagnetic dispersion relation (solid line), and as obtained from TORIC (dashed line).

the ICW rather than the IBW. Figure 4(b) shows the power deposited into the plasma from the ICW. This is calculated using the imaginary part of $n_\perp$ obtained by solving the full electromagnetic dispersion relation and Eq. (1) (shown by the solid line), and compared to the TORIC results (dashed line). The power deposited by the IBW is found to be a small fraction of the absorbed power. In the TORIC simulations for these scenarios, the ICW oscillations are mostly localized along a flux surface, and are located to the low-field side of the mode-conversion layer. Fourier analysis of the E_{RF} solutions indicates that the characteristic m_θ numbers are in the range of 50–80 (positive below the midplane for large positive n_ϕ, negative above the midplane for large negative n_ϕ). These high m_θ numbers are converted to large $n_\parallel$ through the local poloidal field resulting in a propagating solution to the local dispersion relation. A possible explanation for the stark up-down asymmetry in Fig. 4(a) (not as apparent in low n_ϕ simulations) is shown by the difference in the location of the $n_\parallel^2 = S$ layer for the m_θ number characteristic of the ICW in this case: $m = +53$ (curved dotted line reaching to 2.5 cm), and the $n_\parallel^2 = S$ layer for $m = -53$ (curved dashed line reaching to -1 cm), which would be the corresponding m_θ number for an ICW above the midplane. As can be seen in the figure, there is no ICW above the midplane for this n_ϕ. This may be understood by considering a change in the character of this wave on opposite sides of its $n_\parallel^2 = S$ layer [20]. TORIC simulations of D-H plasmas show similar results.

In summary, the mode-converted ICW first derived by Perkins has been observed for the first time in the Alcator C-Mod tokamak with the use of PCI imaging techniques in a H-^{3}He plasma. These waves heat electrons along a magnetic flux surface. This process can be expected to play a role in future D-T burning plasma experiments with ICRF heating because the cyclotron frequency ratio (and hence the wave physics) is the same as for H-^{3}He.

We would like to acknowledge the support of the Alcator C-Mod group, and to thank Dr. Brambilla for the use of the TORIC code. E. N-M. would like to thank Dr. Abhay Ram for many helpful discussions on mode conversion and IBW, and M. P. wishes to thank Dr. F. W. Perkins and Dr. C. K. Phillips for stimulating discussions. This work is supported by U.S. DoE Cooperative Agreement No. DE-FC02-99ER54512.

*Email address: eric.nelson-melby@epfl.ch
Present address: CRPP-EPFL, Lausanne, Switzerland.

[1] K. Budden, *Radio Waves in the Ionosphere* (Cambridge University Press, Cambridge, U.K., 1961).
[2] T. H. Stix, *Waves in Plasmas* (American Institute of Physics, New York, 1992).
[3] F. W. Perkins, Nucl. Fusion **17**, 1197 (1977).
[4] R. Majeski, C. K. Phillips, and J. R. Wilson, Phys. Rev. Lett. **73**, 2204 (1994).
[5] C. N. Lashmore-Davies, V. Fuchs, A. K. Ram, and A. Bers, Phys. Plasmas **4**, 2031 (1997).
[6] I. Monakhov, A. Bécoulet, D. Fraboulet, and F. Nguyen, Phys. Plasmas **6**, 885 (1999).
[7] A. Jaun, T. Hellsten, and S. C. Chiu, Nucl. Fusion **38**, 153 (1998).
[8] E. F. Jaeger *et al.*, Phys. Plasmas **8**, 1573 (2001).
[9] M. Brambilla, Plasma Phys. Controlled Fusion **41**, 1 (1999).
[10] P. Lee *et al.*, Phys. Rev. Lett. **49**, 205 (1982).
[11] H. Park, N. C. Luhmann, Jr., W. A. Peebles, and R. Kirkwood, Phys. Rev. Lett. **52**, 1609 (1984).
[12] T. F. R. Group, A. Truc, and D. Gresillon, Nucl. Fusion **22**, 1577 (1982).
[13] J. Hosea *et al.*, in *Proceedings of the 4th International Symposium on Heating in Toroidal Plasmas, Rome, 1984*, edited by H. Knoepfel and E. Sindoni (ENEA, Rome, 1984), Vol. I, pp. 261–275.
[14] H. Weisen, Rev. Sci. Instrum. **59**, 1544 (1988).
[15] S. Coda, M. Porkolab, and T. N. Carlstrom, Rev. Sci. Instrum. **63**, 4974 (1992).
[16] I. H. Hutchinson *et al.*, Phys. Plasmas **1**, 1511 (1994).
[17] E. Nelson-Melby, A. Mazurenko, M. Porkolab, P. T. Bonoli, and S. J. Wukitch, in *14th Topical Conference on Radio Frequency Power in Plasmas*, edited by T. K. Mau and J. deGrassie, AIP Conf. Proc. No. 595 (AIP, New York, 2001), pp. 90–97.
[18] E. Nelson-Melby *et al.*, in *Proceedings of the 29th European Physical Society Conference on Plasma Physics and Controlled Fusion, Montreux, Switzerland, 2002* (IOP, Bristol, U.K., 2002).
[19] E. Nelson-Melby, Ph.D. thesis, Massachusetts Institute of Technology, 2001 (http://www.psfc.mit.edu/library/01rr/01RR006/01RR006_ABS.HTML).
[20] M. Brambilla, *Kinetic Theory of Plasma Waves* (Clarendon Press, Oxford University, 1998).